



OPEN

# Electromagnetic Wave Absorbing Properties of Amorphous Carbon Nanotubes

SUBJECT AREAS:  
CARBON NANOTUBES  
AND FULLERENES

SYNTHESIS AND PROCESSING

Received  
17 April 2014Accepted  
20 June 2014Published  
10 July 2014Correspondence and  
requests for materials  
should be addressed to  
T.K.Z. (ztk-xjtu@163.  
com)Tingkai Zhao<sup>1</sup>, Cuilin Hou<sup>1</sup>, Hongyan Zhang<sup>1</sup>, Ruoxing Zhu<sup>1</sup>, Shengfei She<sup>1</sup>, Jungao Wang<sup>1</sup>, Tiehu Li<sup>1</sup>, Zhifu Liu<sup>2</sup> & Bingqing Wei<sup>1,3</sup><sup>1</sup>School of Materials Science and Engineering, Northwestern Polytechnical University, Xi'an 710072, P. R. China, <sup>2</sup>Department of Materials Science and Engineering, Northwestern University, Evanston IL 60208, USA, <sup>3</sup>Department of Mechanical Engineering, University of Delaware, Newark DE 19716, USA.

Amorphous carbon nanotubes (ACNTs) with diameters in the range of 7–50 nm were used as absorber materials for electromagnetic waves. The electromagnetic wave absorbing composite films were prepared by a dip-coating method using a uniform mixture of rare earth lanthanum nitrate doped ACNTs and polyvinyl chloride (PVC). The microstructures of ACNTs and ACNT/PVC composites were characterized using transmission electron microscope and X-ray diffraction, and their electromagnetic wave absorbing properties were measured using a vector-network analyzer. The experimental results indicated that the electromagnetic wave absorbing properties of ACNTs are superior to multi-walled CNTs, and greatly improved by doping 6 wt% lanthanum nitrate. The reflection loss (*R*) value of a lanthanum nitrate doped ACNT/PVC composite was −25.02 dB at 14.44 GHz, and the frequency bandwidth corresponding to the reflector loss at −10 dB was up to 5.8 GHz within the frequency range of 2–18 GHz.

Radar stealth technology is used to decrease the radar cross section (RCS) by the weakening, absorption, and deflection of a target radar wave and it is difficult to be identified and discovered by the source radar within a frequency range. One of the technological approaches is to make use of radar absorbing materials (RAMs) to decrease the RCS of a target source. At present, novel RAMs with nanometer-sized stealth features are being gradually used as alternatives of conventional stealth materials. These new RAMs could meet the requirements for the next generation radar stealth equipment, namely, light weight, thin thickness, powerful absorption, and wide frequency bandwidth (the main characteristics of new electromagnetic wave absorbing materials: “Light, Thin, Strong, and Wide”)<sup>1,2</sup>.

Carbon nanotubes (CNTs)<sup>3</sup> are the most representative 1D nanoscale materials. CNTs can be divided into two types based on their crystalline structures: crystalline CNTs and amorphous CNTs (ACNTs). CNTs have extremely high mechanical strength and toughness, good electrical conductivity, excellent thermal conductivity, and electromagnetic wave absorbing properties<sup>4–6</sup>. For the electromagnetic wave absorbing field, CNTs possess the advantages of light weight, good compatibility, and wide frequency bandwidth<sup>7,8</sup>. Thus, CNT is a promising material for next-generation nanoscale electromagnetic wave absorbing applications. When compared to traditional microwave absorbing materials such as resistance radar-absorbing materials, dielectric absorbing materials, and magnetic medium absorbent materials, CNTs have superior qualities that make them stand out. Recently, many researchers have carried out investigations on the electromagnetic wave absorbing property of CNTs. Ali Ghasemi *et al.*<sup>9–11</sup> reported that ferrite/CNT composites have good microwave absorbing properties, with a frequency bandwidth of 6 GHz and a reflection loss below −10 dB at the frequency range of 12–18 GHz. S. Sutrardhar *et al.*<sup>12,13</sup> studied the microwave absorption of ferrite nanoparticle/CNT composites, and showed a maximum reflection loss of −59 dB at 13.4 GHz in the Ku band. Du *et al.*<sup>14</sup> studied the microwave absorbing properties of as-grown, cobalt electroplated and activated CNTs/epoxy resin composites that have high absorbing strengths and wide frequency bandwidth at the C, X, and Ku frequency bands. In addition, Zhao *et al.*<sup>15</sup> revealed the radar wave absorbing properties of CNTs and carbonyl iron modified CNTs, and the results displayed the maximum reflection loss was −22.89 dB at 11.4 GHz in the frequency range of 2–18 GHz. Cao *et al.*<sup>16</sup> reported that the frequency bandwidth of the absorbing materials, with 8% CNTs corresponding to the reflection loss below −5 dB, was 10.0 GHz at the frequency range of 8–40 GHz. Although all of above mentioned studies have been on the electromagnetic wave absorbing performance of CNTs composites, the development of lightweight



nanocomposites having wide frequency range, bandwidth is still a challenging task for radar wave absorbing applications.

ACNTs<sup>17</sup> have different tube wall structures compared with crystalline CNTs. The tube walls are composed of many discontinuous graphene sheets and carbon clusters, which exhibit features of short-range order and long-range disorder, and have many defects, dangling bonds and huge specific surfaces. Thus, ACNTs are anticipated to have higher electromagnetic wave absorbing properties than crystalline CNTs. This new material as an electromagnetic wave absorber may solve some of the issues in radar wave absorbing applications. In this paper, the microwave absorbing properties of ACNTs as electromagnetic wave absorbers have been studied, which has not been reported before. The exploration is helpful to develop a new generation nanosized stealth material.

## Results

Figure 1 shows the SEM image and corresponding energy dispersive spectroscopy (EDS) spectrum of the  $\text{La}(\text{NO}_3)_3$ -ACNTs. The  $\text{La}(\text{NO}_3)_3$  wrapped ACNTs with a diameter of 50 nm was formed (see Figure 1a). Figure 1a illustrates an interwoven ACNT network consisting of  $\text{La}(\text{NO}_3)_3$  nanoparticles in the composite.  $\text{La}(\text{NO}_3)_3$  nanoparticles are also favorable to limit the aggregation of ACNTs. EDS analysis (see Figure 1b) corresponding to the white rectangle area in Figure 1a indicates that the  $\text{La}(\text{NO}_3)_3$ -ACNTs consists of C, O, and La, confirming that La has been grafted onto the surface of ACNTs.

TEM images of MWCNTs, ACNTs, and  $\text{La}(\text{NO}_3)_3$ -ACNTs are shown in Figure 2. Figure 2a indicates that the MWCNTs show almost no agglomeration after acid treatment and the diameters are about 12 nm. The tube walls are smooth and thin, and the lumen was almost unobstructed. HRTEM of a MWCNT clearly shows the tube wall in the inset image of Figure 2a. Figure 2b shows that the tube walls of the ACNTs are thick, and the diameters range from 10–25 nm. The tubes along the axial direction were not straight and were curved everywhere. Figure 2c shows the tube outer-wall structure of ACNTs made of discontinuous graphene sheets and carbon clusters with short-range order and long-range disorder. The diameter of this nanotube is about 12 nm and the sheet distance between the graphene sheets measured by HRTEM is about 0.368 nm. ACNTs have a unique electronic band structure because they have larger sheet distance than MWCNTs (0.34 nm) and graphite (0.335 nm). The inset image in Figure 2c is the selected area electron diffraction (SAED) pattern of the corresponding nanotubes. The spot- and ring-like patterns indicate that the CNTs have poor crystallinity. Although this CNT has an amorphous feature, the crystal units exist in short-range order structures as shown in Figure 2d. It is similar to the microcrystalline structure (small graphene sheets) with many

defects. Figure 2d shows the open tip of an ACNT (about 19 nm in diameter, and the sheet distance between small graphene sheets or carbon clusters is about 0.363 nm) having metal catalyst nanoparticle (about 11 nm in diameter) with a round or faceted morphology. They are either coated with amorphous carbon shell or naked. The wall thickness of the ACNTs is about 5 nm. The wall thickness of MWCNTs is about 2–20 nm. Therefore, for the same wall thickness, ACNTs have more graphene sheets and carbon clusters than MWCNTs due to the turbine-like tube wall structure. The tube cap was also opened. In Figure 2e, we observe that the surface of hollow ACNTs is rough, and a certain amount of small black particles is attached to the outer surface. These ACNTs have not reunited adequately and have a favorable dispersibility effect. Figure 2f shows  $\text{La}(\text{NO}_3)_3$  grafted on the surfaces of ACNTs. This composite is not pure and contains a certain amount of impurities such as amorphous carbon and carbon balls. EDS analysis (see Figure 2g) corresponding to the blue rectangle area of Figure 2f indicates that the  $\text{La}(\text{NO}_3)_3$ -ACNTs consists of C and La, confirming that La has been grafted onto ACNTs. Co and Ni are from the catalysts for the ACNT preparation, and Cu element is from the copper grid. This EDS result in Figure 2g is in agreement with that of EDS in Figure 1b.

XRD patterns of MWCNTs, ACNTs, and  $\text{La}(\text{NO}_3)_3$ -ACNTs are shown in Figure 3. MWCNTs at 26.3°C (002) have a higher purity, and no impurity particles are detected. The crystal plane diffraction peak of ACNTs at 22°C (002) is very small compared with that of MWCNTs. So the crystallinity of ACNTs is very low. This indicates that the crystal structure of ACNTs is almost amorphous, in agreement with the HRTEM result in Figure 2c & d. The black small particles on the tube wall of  $\text{La}(\text{NO}_3)_3$  doped ACNTs may be  $\text{La}(\text{NO}_3)_3$  nanoparticles (the solid squares in Figure 3) and small amounts of  $\text{La}(\text{OH})_3$  nanoparticles (the solid circles in Figure 3) as  $\text{La}(\text{NO}_3)_3$  hydrolyzed.

The complex permittivity and permeability results of all CNT/PVC composites are shown in Figure 4 at the frequency range of 2–18 GHz. Figure 4a demonstrates the changes in the real part ( $\epsilon'$ ) and imaginary part ( $\epsilon''$ ) of the complex permittivity of all composites vs frequency. With frequency increasing from 2 to 18 GHz, the real and imaginary parts of the complex permittivity slightly decrease except for that of  $\text{La}(\text{NO}_3)_3$  doped ACNT/PVC composite. This may be because the change in the applied electromagnetic field is faster than that of current carriers due to the dispersive character of the rare metal and CNTs<sup>18,19</sup>. When frequency increases, electrons gain higher energy, tunneling effect is also more obvious, and thus the conductivity is influenced<sup>20</sup>. From Figure 4b, it can be seen that the real part ( $\mu'$ ) and imaginary part ( $\mu''$ ) of the complex permeability of all the composites show almost no change with increasing frequency except that of the  $\text{La}(\text{NO}_3)_3$ -ACNT/PVC composite with several

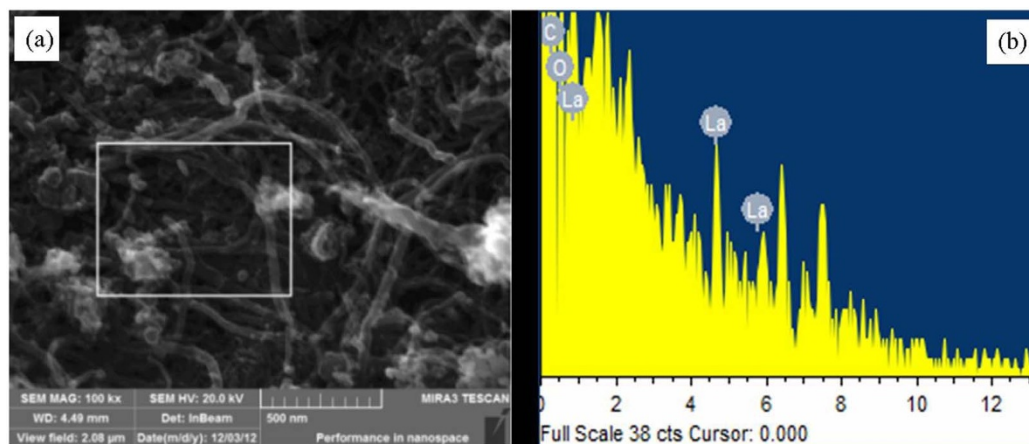


**Figure 1** | SEM image (a) and corresponding EDS spectrum (b) (unit: keV) of  $\text{La}(\text{NO}_3)_3$ -ACNTs.

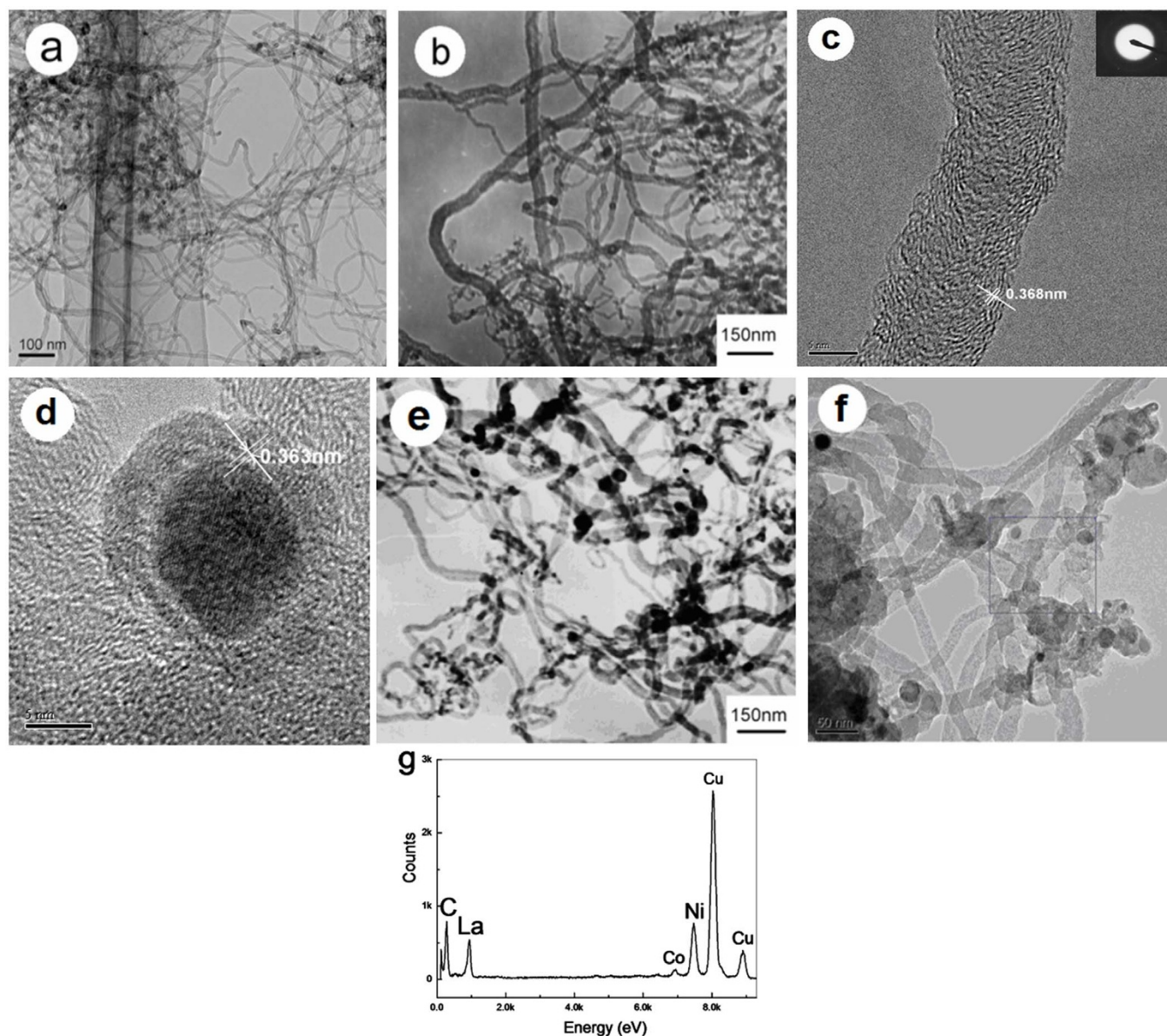


**Figure 2** | TEM images of MWCNTs (a), ACNTs (b)–(d),  $\text{La}(\text{NO}_3)_3$ -ACNTs (e)–(f), and EDX pattern (g).

resonance peaks. This indicates that the magnetic spectrum of  $\text{La}(\text{NO}_3)_3$ -ACNTs/PVC film is a mixture of magnetic resonance and relaxation spectroscopy. The magnetic losses increase due to the resonance peaks. It confirms that the doped rare earth lanthanum element may enhance the magnetic anisotropy and relaxor characteristics of the composite film<sup>21,22</sup>. Therefore, the doping of lanthanum nitrate in the ACNT/PVC composite films plays an important role in the electromagnetic wave absorbing performance.

Based on the data for the electromagnetic parameters ( $\epsilon_r = \epsilon' - j\epsilon''$ ,  $\mu_r = \mu' - j\mu''$ ) from Figure 4, the dielectric dissipation factor ( $\tan\delta_\epsilon$ ) and the magnetic dissipation factor ( $\tan\delta_\mu$ ) were calculated (see Figure 5) at the frequency range of 2–18 GHz. From the comparison of  $\tan\delta$  in Figure 5a and Figure 5b, we see that  $\tan\delta_\epsilon$  of the  $\text{La}(\text{NO}_3)_3$ -ACNT/PVC composite increases sharply with frequency in 2–18 GHz range and it is the largest value in all samples. However, there are two resonance peaks in the  $\tan\delta_\mu$  curve for the  $\text{La}(\text{NO}_3)_3$ -ACNT/PVC composite. One possible reason is that the electrical double layers (EDL) of CNTs in the PVC-THF solution can be compressed by the interactions of interfacial EDL.  $\text{La}^{3+}$  moved on the surface of ACNTs due to diffusion and lead to an increase in the magnetic loss of the composites. The capacity of electromagnetic

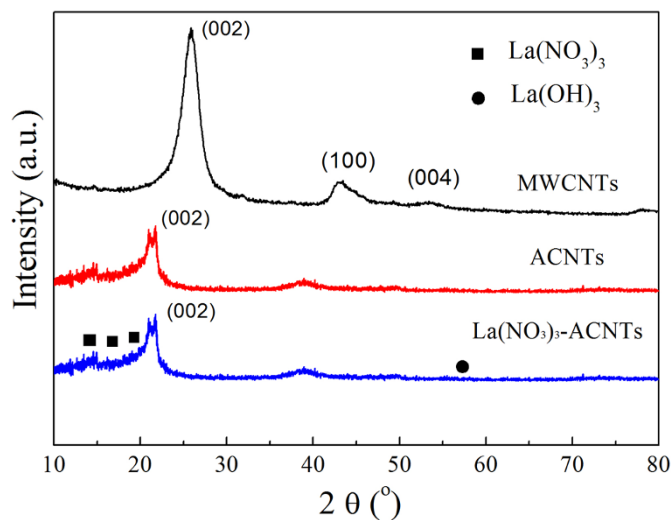


**Figure 3** | XRD patterns of MWCNTs, ACNTs, and  $\text{La}(\text{NO}_3)_3$ -ACNTs.

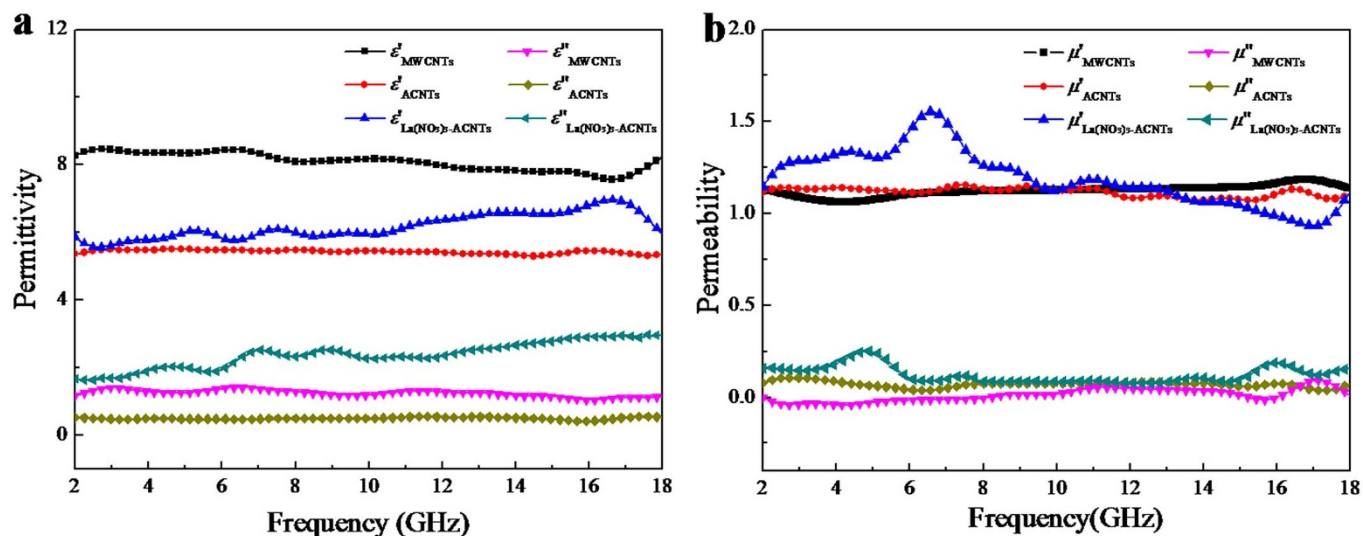


**Figure 4** | Complex permittivity ( $\epsilon'$ ,  $\epsilon''$ ) (a) and permeability ( $\mu'$ ,  $\mu''$ ) (b) spectra of CNT/PVC composite films vs frequency.

absorption can be therefore determined by both the dielectric and magnetic losses.

Figure 6 gives the reflection losses of MWCNT/PVC, ACNT/PVC, and La(NO<sub>3</sub>)<sub>3</sub>-ACNT/PVC composites at the frequency range of 2–18 GHz. Among all the composites, the minimum reflection loss of the MWCNT/PVC composite is the highest and its bandwidth (0.2 GHz) is also the narrowest ( $< -10$  dB). However, the minimum reflection loss of the La(NO<sub>3</sub>)<sub>3</sub>-ACNTs/PVC composite is the lowest and its bandwidth (5.8 GHz) is also the widest ( $< -10$  dB) (see Table 1). This may be attributed to the special tube wall structure of ACNTs. ACNTs have the characteristics of short-range order and long-range disorder, while the degree of graphitization of the tube wall structure is poorer than that of MWCNTs. Therefore, its dielectric and permeability properties increase, resulting in the increase of its dielectric loss and magnetic loss. The doping of lanthanum nitrate in the ACNT/PVC composite films plays the main role in the electromagnetic wave absorbing performance. In addition, a little La(NO<sub>3</sub>)<sub>3</sub> might hydrolyze to generate La(OH)<sub>3</sub> nanoparticles attached to the wall. According to the Kubo theory, the electronic level of La(OH)<sub>3</sub> nanoparticles splits (due to quantum effect) and the split energy level spacing is in the range of the energy of microwaves ( $10^{-2}$ – $10^{-5}$  eV), such that the absorbing effect or channels can be established. Therefore, the performance of ACNTs could be

enhanced due to the absorption of lanthanum nitrate compounds, La<sup>3+</sup> ions, and/or the formation of La(OH)<sub>3</sub> nanoparticles<sup>23</sup>. The results show that the absorbing peak value of the La(NO<sub>3</sub>)<sub>3</sub>-ACNT/PVC composite corresponding to the reflector loss at  $-25.02$  dB is the lowest at 14.44 GHz, and the absorbing bandwidth corresponding to the reflector loss at  $-10$  dB is more than 5.8 GHz.

## Discussion

Recently, immense achievements in the field of electromagnetic absorption of magnetic nanoparticles have been made, especially in the study of the electromagnetic performance of ferrite or other metal doped MWCNT nanocomposites. The weight of nanocomposites based on metal-oxide compounds was found to be higher (e.g. the density of ferrite is 5 g/cm<sup>3</sup>), and the frequency bandwidth was not as broad as that of the composites based on PVC (the density of PVC is 1.37 g/cm<sup>3</sup>) used in this study. In the present work on the ACNT/PVC nanocomposite films, the film weight is very light and the frequency bandwidth is significantly improved. The overall performances are quite high compared to that of other reports.

In general, CNTs have an excellent electromagnetic wave absorption performance due to its unique tube wall structure and outstanding electrical conductivity. Similarly, the important factor for ACNTs to absorb the electromagnetic wave absorption is its excellent

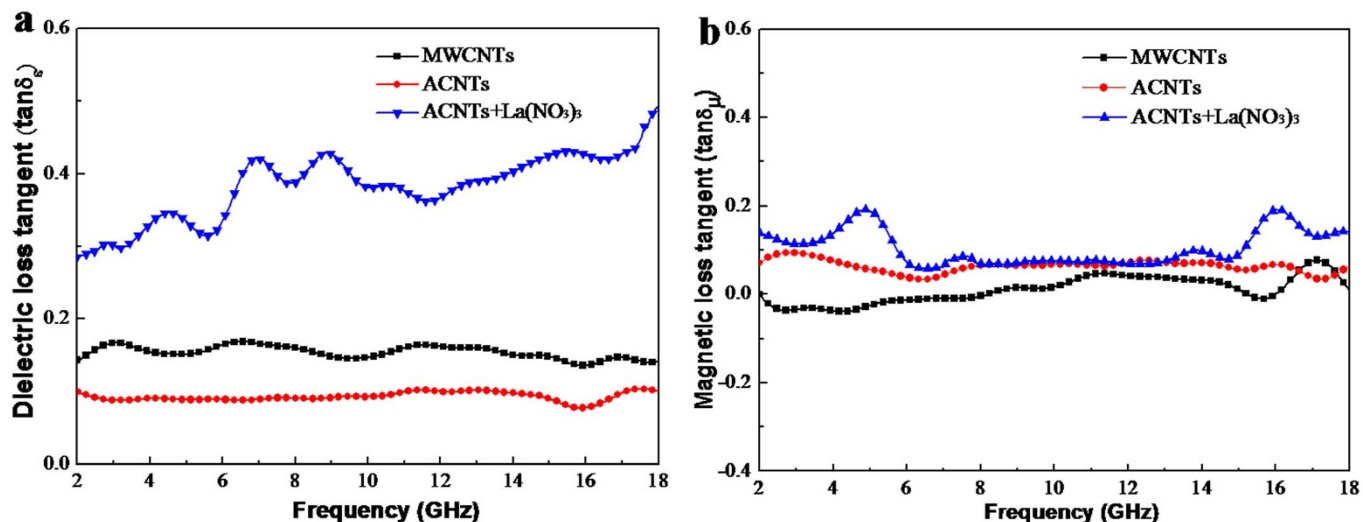


**Figure 5** | Dielectric loss tangent ( $\tan\delta_\epsilon$ ) (a) and magnetic loss tangent ( $\tan\delta_\mu$ ) (b) of CNT/PVC composite films vs frequency.

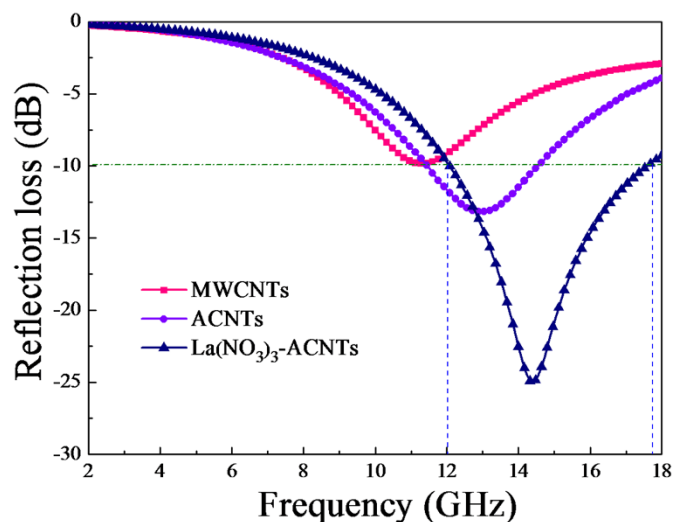


**Figure 6** | Reflection losses of MWCNT/PVC, ACNT/PVC, and  $\text{La}(\text{NO}_3)_3$ -ACNT/PVC composites.

conductivity even though there are many defects on the tube walls. Due to the large aspect ratio, ACNTs easily form conductive networks in the composite films to transfer the electrons. Compared to the tube wall structure of crystalline CNTs, ACNTs not only have short-range order (similar to the crystalline structure of MWCNTs & SWCNTs) but also have long-range disorder (prolongs the propagation path of electromagnetic waves). Therefore, ACNTs have more excellent electromagnetic wave absorbing performance than other CNTs. The mechanism of crystalline CNTs with excellent conductivity to increase the dielectric loss is clear. Here we only discuss how to enhance the electromagnetic wave absorption properties of the ACNTs with long-range disorder structure.

A possible electromagnetic wave absorbing mechanism of ACNTs is schematically depicted in Figure 7. Besides the excellent conductivity for ACNTs to absorb the electromagnetic wave absorption, ACNTs have another unique amorphous structure to increase the electromagnetic wave absorption properties. According to reference 24 and the tube wall structural characteristics of ACNTs<sup>25</sup>, dihedral angles could be easily formed within the graphene sheet stacks of the ACNTs tube walls in the ACNTs/PVC composite. The electromagnetic waves go through multiple reflections from many dihedral angles, and this process prolongs the propagation path of electromagnetic waves in the absorbers. The multiple reflections of microwave lead to the higher losses of electromagnetic energy. It may also be due to the fact the interaction of microwaves with dielectric materials intensified the molecular motions such as ionic conduction, dipolar polarization relaxation, etc. Within the absorber materials, resistive forces in the composites dampen these molecular motions and result in energy dissipation in the form of heat through molecular friction and dielectric loss. The interaction efficiency of molecules with waves and heating of materials depend on the ability of materials to absorb microwaves and convert them into heat. Therefore, these multiple reflections of electromagnetic waves enhanced the thermal conversion efficiency which is proportional to the imaginary part, and it is favorable to the higher losses of electromagnetic energy.

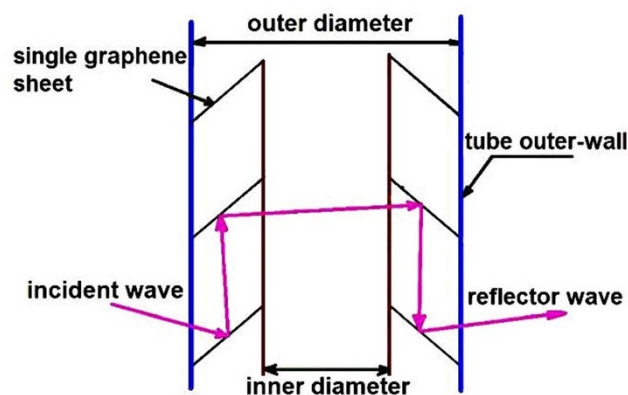
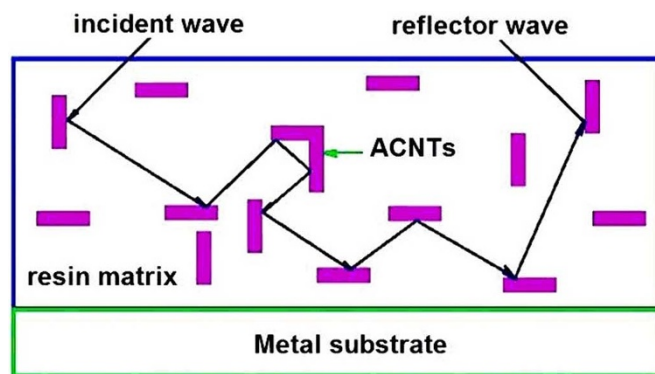


**Figure 7** | Schematics of the electromagnetic wave absorbing mechanism of ACNTs.

ACNTs have more excellent electromagnetic wave absorbing properties than crystalline CNTs due to their unique structures. The possible reasons for their excellent absorbing properties are: (a) ACNTs have different tube wall structures compared with crystalline CNTs. The tube wall is composed of many graphene sheets and or carbon clusters, which exhibit the features of short-range order and long-range disorder. The features of short-range order lead to the microcrystalline structure with many defects of ACNTs which makes the dielectric loss increase significantly due to its excellent conductivity. The features of long-range disorder lead to the worse crystallinity of ACNTs which makes the complex permeability increase significantly and sharply improved the electromagnetic wave absorbing property. The feature of the short-range order may provide many channels for the electromagnetic wave absorption. (b) The outside tube-wall of ACNTs is jagged and has many defects, dangling bonds, and huge specific surface. They are all contributing to the enhancement of the electromagnetic wave absorption. (c) Many dangling bonds that exist give rise to the interfacial polarization and huge specific surface could cause multiple scattering effects. So the electromagnetic wave absorbing property increased dramatically. (d) ACNTs have an obvious electroresistive effect due to their unique tube-wall structures. The impedance of ACNTs should come near to the impedance of free space, and they matched very well to each other.

**Table 1** | Electromagnetic wave absorbing properties of CNT/PVC composite films

Samples	Film thickness (mm)	Reflection loss (dB)	Frequency (GHz)	Frequency bandwidth (GHz)
MWCNTs	2	-10	11.32	0.2
ACNTs	2	-13.20	12.96	3.3
$\text{La}(\text{NO}_3)_3$ -ACNTs	2	-25.02	14.44	5.8



In summary, ACNT/PVC composite films with a thickness of 2 mm were prepared by dip-coating method using  $\text{La}(\text{NO}_3)_3$  doped ACNTs as absorbers. The microwave absorbing property of the  $\text{La}(\text{NO}_3)_3$  doped ACNTs was greatly improved. We demonstrated that ACNTs have more excellent electromagnetic wave absorption property than that of MWCNTs. The reflection loss value of CNTs/PVC with a matching thickness of 2 mm increased from  $-13.20$  to  $-25.02$  dB, the frequency bandwidth corresponding to the reflector loss at  $-10$  dB increased from 3.3 to 5.8 GHz, and the position of absorbing peak shifted from 12.96 to 14.44 GHz. ACNTs could effectively improve the electromagnetic wave absorbing properties of the composites at the frequency range of 2–18 GHz.

## Methods

**Materials.** As-grown ACNTs were prepared by a temperature-controlled arc discharging furnace<sup>26,27</sup> in a hydrogen gas at 600°C, and Co-Ni alloy powders were used as catalysts. The production quantity and purity reached 8 g/h and 80%, respectively. The diameter of the as-grown ACNTs is in the range of 7–60 nm.

**Synthesis of CNT/PVC composites.** ACNTs and MWCNTs (purity: >95%, average diameter: 20 nm, Tsinghua University, China) were ultrasonically treated for 4 hrs with a mixture of concentrated acid ( $\text{HNO}_3$ :  $\text{H}_2\text{SO}_4 = 1:3$ , v/v) to increase their purity and activity. The acid-treated ACNTs or MWCNTs were grounded for 1 h, and ultrasonically agitated at 25°C for 1 h with 6 wt.%  $\text{La}(\text{NO}_3)_3$  (Zibo Qilin Chemical Plant, China) in ethanol solution, then dried at 80°C for 5 h in an oven, and finally ground for 30 min. Polyvinyl chloride (PVC) powder (SG-7, Xi'an Chemical Plant, China) was dissolved in tetrahydrofuran (THF, Shanghai Tongshi Chemical Co., Ltd., China) under stirring to form a 16% w/v solution, followed by adding MWCNTs, dioctyl phthalate (DOP, Tianjin Chemical Reagent Factory, China) ( $w_{\text{ACNTs(or MWCNTs)}}:w_{\text{DOP}}:w_{\text{PVC}} = 8:3:100$ ) and a small amount of crosslinking agent (styrene, ~1.5 wt.%, Tianjin Fuchen Chemical Reagent Factory, China). The ACNT (or MWCNT)/PVC composite films (the thickness is 2 mm) were prepared by a dip-coating method using the above resulting mixtures. The composite specimens were placed in a doughnut-shaped ( $\Phi_{\text{out}}: 7.03$  mm,  $\Phi_{\text{in}}: 3.00$  mm) mold and dried for 24 hrs in air. Finally, ACNTs modified PVC resin based composites were prepared. Similarly, MWCNT/PVC and  $\text{La}(\text{NO}_3)_3$ -ACNT/PVC composites were prepared by the same technical process. The additive content of MWCNTs in MWCNTs/PVC and ACNTs in ACNTs/PVC composites was all 8.0 wt%, and the additive content of  $\text{La}(\text{NO}_3)_3$  and ACNTs in  $\text{La}(\text{NO}_3)_3$ -ACNTs/PVC composite was 0.5 wt% and 7.5 wt% respectively.

**Characterization.** The microstructures of MWCNTs, ACNTs and  $\text{La}(\text{NO}_3)_3$ -ACNTs were observed by using a transmission electron microscope (TEM, JEM-100CXII, JEOL). X-ray diffraction (XRD, X'PertPro, PANalytical) patterns were used to identify the phase structure of ACNTs, MWCNTs, and  $\text{La}(\text{NO}_3)_3$ -ACNTs with  $\text{Cu K}_\alpha$  radiation.

**Electromagnetic parameter measurements.** The real and imaginary parts of the complex permittivity ( $\epsilon'$ ,  $\epsilon''$ ) and permeability ( $\mu'$ ,  $\mu''$ ) of the CNT composites were measured by a MS4644A Vector-network Analyzer (Anritsu: 10 MHz–40 GHz)<sup>28</sup>. According to the transmission theory, for a single-layer absorber composite, the reflection loss (R) can be calculated from the equations shown below<sup>29</sup>.

$$R(\text{dB}) = 20 \log_{10} \left| \frac{Z_{\text{in}} - 1}{Z_{\text{in}} + 1} \right|, \quad (1)$$

$$Z_{\text{in}} = \sqrt{\frac{\mu_r}{\epsilon_r}} \tanh \left[ j \left( \frac{2\pi f d}{c} \right) \sqrt{\mu_r \epsilon_r} \right] \quad (2)$$

Where  $Z_{\text{in}}$  is the normalized input impedance at free space and material interface,  $\epsilon_r = \epsilon' - j\epsilon''$  is the complex permittivity, and  $\mu_r = \mu' - j\mu''$  is the complex permeability of absorbers,  $f$  is the frequency of the microwave in free space,  $d$  is the thickness of the absorber, and  $c$  is the velocity of light in free space. The impedance matching condition is given by  $Z_{\text{in}} = 1$  to represent the perfect absorbing properties. The impedance matching condition is determined by the combinations of six parameters,  $\epsilon'$ ,  $\epsilon''$ ,  $\mu'$ ,  $\mu''$ ,  $f$  and  $d$ , the reflection loss curve versus frequency can be calculated at a specified thickness from  $\epsilon_r$  and  $\mu_r$ .

1. Vinoy, K. J. & Jha, R. M. *Radar Absorbing Materials: From Theory to Design and Characterization* (Boston, 1996).
2. Qin, F. & Brosseau, C. A review and analysis of microwave absorption in polymer composites filled with carbonaceous particles. *J. Appl. Phys.* **111**, 061301-1-24 (2012).
3. Iijima, S. Helical microtubules of graphitic carbon. *Nature* **354**, 56–58 (1991).
4. O'Connell, M. J. *Carbon Nanotubes Properties and Applications* (Boca Raton, 2006).

5. Jiang, W. *et al.* Superparamagnetic cobalt-ferrite-modified carbon nanotubes using a facile method. *Mater. Sci. Eng. B.* **166**, 132–134 (2010).
6. Ye, Z. *et al.* Electromagnetic wave absorption properties of carbon nanotubes-epoxy composites at microwave frequencies. *J. Appl. Phys.* **108**, 054315-1-7 (2010).
7. Qi, X. S. *et al.* Large-scale synthesis, characterization and microwave absorption properties of carbon nanotubes of different helicities. *J. Solid State Chem.* **182**, 2691–2697 (2009).
8. Ren, F. J. *et al.* Current progress on the modification of carbon nanotubes and their application in electromagnetic wave absorption. *RSC Adv.* **4**, 14419–14431 (2014).
9. Ghasemi, A. Remarkable influence of carbon nanotubes on microwave absorption characteristics of strontium ferrite/CNT nanocomposites. *J. Magn. Magn. Mater.* **323**, 3133–3137 (2011).
10. Ghasemi, A. *et al.* Enhanced reflection loss characteristics of substituted barium ferrite/functionalized multi-walled carbon nanotube nanocomposites. *J. Appl. Phys.* **109**, 07A507 (2011).
11. Ghasemi, A. *et al.* A comparison between magnetic and reflection loss characteristics of substituted strontium ferrite and nanocomposites of ferrite/carbon nanotubes. *J. Appl. Phys.* **111**, 07B543 (2012).
12. Sutradhar, S. *et al.* Modulated magnetic property, enhanced microwave absorption and Mössbauer spectroscopy of  $\text{Ni}_{0.40}\text{Zn}_{0.40}\text{Cu}_{0.20}\text{Fe}_2\text{O}_4$  nanoparticles embedded in carbon nanotubes. *J. Alloys Comp.* **576**, 126–133 (2013).
13. Sutradhar, S. *et al.* Magnetic and enhanced microwave absorption properties of nanoparticles of  $\text{Li}_{0.32}\text{Zn}_{0.26}\text{Cu}_{0.1}\text{Fe}_{2.32}\text{O}_4$  encapsulated in carbon nanotubes. *Mater. Lett.* **95**, 145–148 (2013).
14. Du, B. *et al.* Microwave absorbing property of MWNTs/epoxy composites. *J. Nanchang Univ., Nat. Sci.* **32**, 439–442 (2008).
15. Zhao, D. L. & Shen, Z. M. Preparation and microwave absorbing properties of microwave absorbing materials containing carbon nanotubes. *J. Inorg. Mater.* **20**, 608–612 (2005).
16. Cao, M. S. *et al.* Research on microwave absorptivity towards CNTs/polyester composites. *J. Mater. Eng.* (Beijing, China) **2**, 34–36 (2003).
17. Zhao, T. K. *et al.* Gas and pressure effects on the synthesis of amorphous carbon nanotubes. *Chin. Sci. Bull.* **49**, 2569–2571 (2004).
18. Hou, C. L. *et al.* Microwave absorption and mechanical properties of  $\text{La}(\text{NO}_3)_3$ -doped multi-walled carbon nanotube/polyvinyl chloride composites. *Mater. Lett.* **67**, 84–87 (2012).
19. Hou, C. L. *et al.* Electromagnetic wave absorbing properties of carbon nanotubes doped rare metal/pure carbon nanotubes double-layer polymer composites. *Mater. Des.* **33**, 413–418 (2012).
20. Duan, Y. P. *et al.* Absorbing properties of  $\alpha$ -manganese dioxide/carbon black double-layer composites. *J. Phys. D: Appl. Phys.* **41**, 125403-1-6 (2008).
21. Russat, J. *et al.* A study of complex permeability in rare earth-substituted cobalt/nonmagnetic transition metal amorphous thin films. *J. Appl. Phys.* **73**, 5592–5594 (1993).
22. Meena, R. S. *et al.* Complex permittivity, permeability and wide band microwave absorbing property of  $\text{La}^{3+}$  substituted U-type hexaferrite. *J. Magn. Magn. Mater.* **322**, 1923–1928 (2010).
23. Xu, J. J. *et al.* Electromagnetic and microwave absorbing properties of  $\text{Co}_2\text{Z}$ -type hexaferrites doped with  $\text{La}^{3+}$ . *J. Magn. Magn. Mater.* **321**, 3231–3235 (2009).
24. Singh, V. K. *et al.* Microwave absorbing properties of a thermally reduced graphene oxide/nitrile butadiene rubber composite. *Carbon* **50**, 2202–2208 (2012).
25. Zhao, T. K. *et al.* Physical model for the growth of amorphous carbon nanotubes. *Appl. Phys. Lett.* **98**, 163111 (2011).
26. Liu, Y. N. *et al.* Amorphous carbon nanotubes produced by a temperature controlled DC arc discharge. *Carbon* **42**, 1852–1855 (2004).
27. Zhao, T. K. *et al.* Temperature and catalyst effects on the production of amorphous carbon nanotubes by a modified arc discharge. *Carbon* **43**, 2907–2912 (2005).
28. Kong, L. *et al.* Electromagnetic wave absorption properties of ZnO-based materials modified with  $\text{ZnAl}_2\text{O}_4$  nanograins. *J. Phys. Chem. C* **117**, 2135–2146 (2013).
29. Zou, T. C. *et al.* Electromagnetic and microwave absorbing properties of multi-walled carbon nanotubes filled with Ni nanowire. *J. Alloys Comp.* **496**, L22–L24 (2010).

## Acknowledgments

This work was supported by the Specialized Research Fund for the Doctoral Program of Higher Education (20096102120016), the Innovation Fund of China Aerospace Science and Technology (CASC200906), the Supporting Program of China Aerospace Science and Technology (CASC201209), the Key Science and Technology Program of Shaanxi Province, China (2013K09-03), and the “111” Project (B08040). B.Q. Wei is grateful for the financial support from the Research Fund of the State Key Laboratory of Solidification Processing (83-TZ-2013).

## Author contributions

T.K.Z. and C.L.H. designed the experiments. C.L.H., H.Y.Z., R.X.Z., S.F.S. and J.G.W. prepared all the samples and carried out characterization and measurement. T.K.Z., C.L.H.



and T.H.L. contributed to the analysis and discussion for the results. T.K.Z., C.L.H., Z.F.L. and B.Q.W. wrote and polished the paper. All authors discussed the results and commented on the manuscript.

### Additional information

**Competing financial interests:** The authors declare no competing financial interests.

**How to cite this article:** Zhao, T. *et al.* Electromagnetic Wave Absorbing Properties of Amorphous Carbon Nanotubes. *Sci. Rep.* 4, 5619; DOI:10.1038/srep05619 (2014).



This work is licensed under a Creative Commons Attribution-NonCommercial-NoDerivs 4.0 International License. The images or other third party material in this article are included in the article's Creative Commons license, unless indicated otherwise in the credit line; if the material is not included under the Creative Commons license, users will need to obtain permission from the license holder in order to reproduce the material. To view a copy of this license, visit <http://creativecommons.org/licenses/by-nc-nd/4.0/>